J. Ocean Univ. China (Oceanic and Coastal Sea Research)
https://doi.org/10.1007/s11802-019-3975-6
ISSN 1672-5182, 2019 18 (5): 1041-1050
http://www.ouc.edu.cn/xbywb/
E-mail:xbywb@ouc.edu.cn

Simulation Study of Potential Impacts of Tidal Farm in the Eastern Waters of Chengshan Cape, China

LIU Xiaodong[1)], YUAN Peng[1), 2), *], WANG Shujie[1), 2)], YUAN Shuai[1)], TAN Junzhe[1), 2)], and SI Xiancai[1), 2)]

1) *College of Engineering*, *Ocean University of China*, *Qingdao* 266100, *China*
2) *Ocean Engineering Key Laboratory of Qingdao*, *Qingdao* 266100, *China*

(Received August 2, 2018; revised April 28, 2019; accepted June 21, 2019)

Abstract The sea area east of Chenshan Cape has peak tidal current flows that exceed 2.3 m s^{-1}, which make it a promising site for the development of tidal current energy. Before these resources can be exploited, a comprehensive assessment is needed of the potential environmental impacts of the extraction of this energy. In this paper, we describe our construction of a three-dimensional hydrodynamic model of the waters near Chengshan Cape, and verify the performance of the model using continuous data measured *in situ*. We modeled the potential impacts of the exploitation of these resources on the flow field by adding a momentum loss term in the governing equation of the model. Simulation results show that an assumed tidal farm with an estimated power output of 20.34 MW would have a significant impact on the surrounding water level, especially next to the farm, where fluctuation could reach 6 cm. The maximum drop in the flow velocity in the wake of the farm was predicted to be more than 0.8 m s^{-1}, and this influence would extend 10 km downstream.

Key words tidal current energy impact; tidal farm; Chenshan Cape; hydrodynamics model; Delft 3D

1 Introduction

In recent years, tidal current energy has been regarded as a promising option for coastal countries for addressing energy shortages and climate change. Many countries have made concerted efforts to develop tidal-current-energy technologies (Feldman, 2007; Defne *et al.*, 2011; Neill *et al.*, 2017). Before this energy can be exploited, initial steps must be taken with respect to resources assessment, the identification of sites for deploying turbine arrays, and environmental impact assessments.

In China, a number of studies on tidal current energy have been conducted in various domestic waters (Li *et al.*, 2012; Chen *et al.*, 2013; Fang *et al.*, 2015; Wu *et al.*, 2017; Li *et al.*, 2018). Among these, the sea area near Chenshan Cape has been identified as a potential site for exploiting these resources in northern China and has been a research hotspot for the assessment of extractable energy.

Chengshan Cape (Fig.1) is situated at the easternmost part of the Shandong Peninsula, China. In its eastern waters, the tide is irregular semi-diurnal, with a flow velocity of more than 2.3 m s^{-1} in certain areas during spring. Its topography is relatively flat and the water depth ranges between 35 m and 80 m. Around the sea area, Wu *et al.* made a preliminary assessment of the tidal current energy in 2010 based on measured data, and then in 2013 these authors evaluated the extractable energy and the impact of energy extraction based on a two-dimensional (2D) hydrodynamics model built by FVCOM. According to their research results, the extractable energy of the cape is 17.9 MW, and the water level may be affected by this energy extraction, with a maximum change of less than 4 cm. In 2012, Yang *et al.* built a three-dimensional (3D) hydrodynamics model based on the Delft 3D model and used the Flux method to assess the resource reserves of the tidal current energy. Their research results showed that the resource reserves are about 122.85 MW, of which 18.43 MW are extractable. In 2013, Li *et al.* studied the temporal and spatial distributions of this energy based on a 3D model built by ECOMSED. According to their simulation results, the average energy density is lower in spring and autumn, higher in summer, and maximum in winter, with the maximum local energy density exceeding 4 kW m^{-2}. Based on the reviewed literature, we found studies of the waters nearby Chengshan Cape to have focused more on the assessment of resource reserves, with few studies focused on the impacts of energy extraction on the surrounding waters.

To determine the volume of tidal current energy resources that could be exploited and the potential influence of any action taken to extract energy in the area, we conducted numerical simulations of a presumed tidal farm using a 3D hydrodynamic model of the sea area based on

* Corresponding author. E-mail: yuanpeng50@hotmail.com

Table 2 Tidal characteristics at each site

Site	During flood tide				During ebb tide				Average velocity ($\mathrm{m\,s^{-1}}$)
	Maximum velocity ($\mathrm{m\,s^{-1}}$)	Average velocity ($\mathrm{m\,s^{-1}}$)	Average direction (°)	Tidal duration (h)	Maximum velocity ($\mathrm{m\,s^{-1}}$)	Average velocity ($\mathrm{m\,s^{-1}}$)	Average direction (°)	Tidal duration (h)	
2-1	1.33	0.81	167	5.38	1.97	1.12	22	7.12	0.97
2-2	1.50	0.83	195	5.38	2.09	1.26	34	7.12	1.08
3-1	1.46	0.86	211	5.25	1.87	1.19	44	7.25	1.07
3-2	1.45	0.73	218	5.46	1.74	1.11	36	7.04	0.96
4-1	1.28	0.77	278	5.50	1.84	1.19	124	7.00	1.01

$$\frac{\partial \zeta}{\partial t}+\frac{\partial\left[(d+\zeta)U\right]}{\partial x}+\frac{\partial\left[(d+\zeta)V\right]}{\partial y}=Q\,. \qquad (1)$$

Transport equation:

$$\frac{\partial(\zeta+d)c}{\partial t}+\frac{\partial(\zeta+d)Uc}{\partial x}+\frac{\partial(\zeta+d)Vc}{\partial y}= D_h\nabla^2 c-\lambda_d\left(d+\zeta\right)c+R\,. \qquad (2)$$

Momentum conservation equation:

$$\frac{\partial U}{\partial t}+U\frac{\partial U}{\partial x}+V\frac{\partial U}{\partial y}-fV= -g\frac{\partial \zeta}{\partial x}-\frac{g}{\rho_0}\int_{-d}^{\zeta}\frac{\partial \rho'}{\partial x}\mathrm{d}z+\frac{\tau_{sx}-\tau_{bx}}{\rho_0\left(d+\zeta\right)}+v_h\nabla^2 U\,, \qquad (3)$$

$$\frac{\partial U}{\partial t}+U\frac{\partial U}{\partial x}+V\frac{\partial U}{\partial y}+fU= -g\frac{\partial \zeta}{\partial y}-\frac{g}{\rho_0}\int_{-d}^{\zeta}\frac{\partial \rho'}{\partial y}\mathrm{d}z+\frac{\tau_{sy}-\tau_{by}}{\rho_0\left(d+\zeta\right)}+v_h\nabla^2 V\,, \qquad (4)$$

where ζ is the water level, d is the water depth relative to a reference plane, U and V are the velocity vector in the x and y directions, respectively, Q is the intensity of mass sources per unit area, f is the Coriolis parameter, v_h is the kinematic horizontal eddy viscosity, ρ_0 is the reference density, ρ' is the anomaly density, τ_{sx} and τ_{sy} are the components of the wind stress acting on the sea surface, τ_{bx} and τ_{by} denote the components of shear stress at the bottom, c is salinity or temperature, D_h is the horizontal eddy diffusivity, λ_d is the first-order decay process, and R is the source term per unit area.

2.2.2 Model building

We adopted a nested-grid modeling approach to reduce overall computation costs while retaining sufficient resolution in the local area under study. Grids with different resolutions (Fig.3(a)) were used for the large and localized regional sea areas, respectively. For a large sea area, we set the resolution of the coarse grid to 700 m to match the resolution of the bathymetric data, with the number of grids being 290×290. For the localized area, we refined the horizontal grid resolution to 50–200 m (Fig.3(b)) (which numbered 599×631) and sliced the flow field by depth into 10 sigma layers, which is considered sufficient to reflect the spatial distribution of the tidal field. The above grids were interpolated with bathymetric data from an electronic chart to obtain a topographic model of the current waters. In addition, to increase the accuracy of the simulation, we calculated the vertical eddy viscosity using the k-ε method.

As boundary conditions for the model of the large sea area, we set the harmonic constants of eight major astronomical tidal constituents (M_2, S_2, N_2, K_2, K_1, O_1, P_1, Q_1)

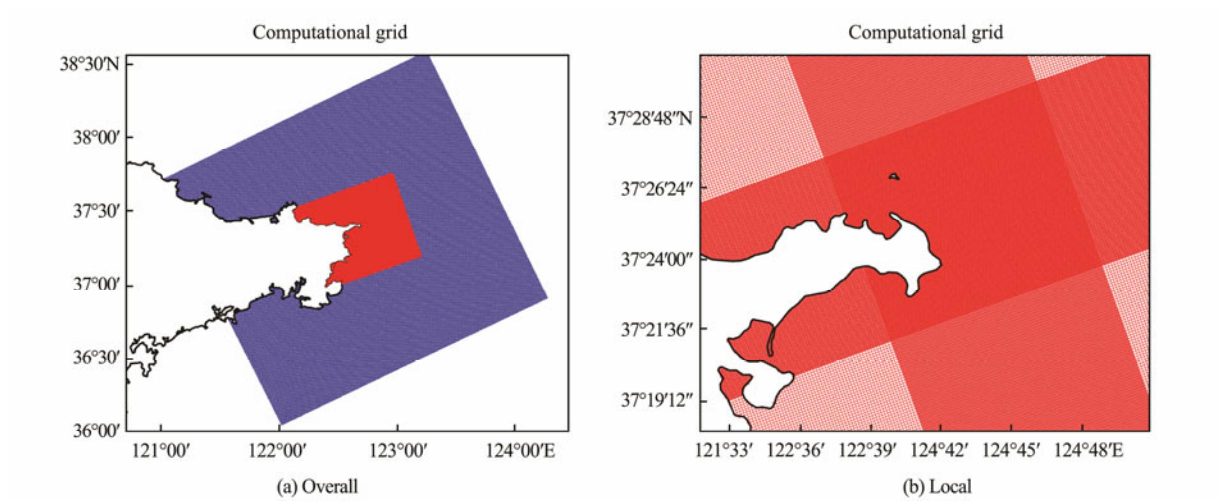

Fig.3 Computational grid. Blue and red areas are the computational grids for the large and localized regions, respectively; the black line indicates the coastline.

at the edge of the computational grid. We then used the time-varying water levels obtained in the grids for the large sea area as the input conditions for calculating the grids for the localized region. The calculation time steps for the large and localized sea areas were 1.0 min and 0.1 min, respectively, which satisfied the Courant condition to ensure computational stability. The simulation covered a period of 32 days from November 30, 2010 to January 1, 2011, including a spin-up time of two days, without considering the effects of wave, wind, and sediment transport.

2.3 Model Verification

2.3.1 Water level verification

To verify the model, we applied harmonic analysis to the simulation results of the water-level time series and the tidal-harmonic-constant data obtained at three measurement points (Fig.1) in the waters near Chengshan Cape (37˚23´37´´N, 122˚41´58´´E), Liugong Island (37˚30´8.81´´N, 122˚11´5.90´´E), and Kongtong Island (37˚33´42.91´´N, 121˚30´50.44´´E).

As shown in Table 3, the simulation results agree well with the data obtained at the measurement points, and the model readily and accurately reproduced the amplitude and phase of the major astronomical tidal constituents.

2.3.2 Flow velocity verification

We also compared the flow velocities obtained at the five sites listed in Table 1 with those obtained in the simulation (Fig.4). To perform this analysis, we used two statistical parameters: root mean square error (RMSE) and correlation coefficient (r), respectively, the calculation formulas for which are as follows:

$$RMSE = \sqrt{\frac{1}{N}\sum_{n=1}^{N}\left(S_n - M_n\right)^2}\ , \tag{5}$$

$$r = \frac{\frac{1}{N}\sum_{n=1}^{N}(S_n - \overline{S_n})(M_n - \overline{M_n})}{\sigma_S \sigma_M}\ , \tag{6}$$

where N is the number of samples, n is the serial number of the data, S_n is the simulated data, M_n is the measured data, and σ_S and σ_M are the standard deviations of the simulated and measured data, respectively.

We found there to be good agreement between the time series of the simulated and measured data (Table 4). However, the flow-velocity simulation results were slightly slower, and there was some degree of error in the flow direction during ebb tide, which may be due to the values set for the model parameters, such as the bottom friction coefficient, topographic resolution, and other parameter, or the fact of having ignored the influence of factors such as wind, waves, and sediment transport.

Overall, despite these few deviations, the model can be used to effectively predict the distribution of tidal currents in these waters.

Table 3 Verification of harmonic constants

Location	Tidal constituents	Measured amplitude (m)	Simulated amplitude (m)	Amplitude deviation (m)	Measured phase lag (˚)	Simulated phase lag (˚)	Phase lag deviation (˚)
Chengshan Cape	M_2	0.34	0.343	−0.003	1	0.9	0.1
	S_2	0.11	0.103	0.007	67	69.4	−2.4
	K_1	0.24	0.237	0.003	315	313.8	1.2
	O_1	0.16	0.161	−0.001	264	260.2	3.8
Liugong Island	M_2	0.59	0.662	−0.072	303	306.5	−3.5
	S_2	0.18	0.184	−0.004	358	2.24	−5.24
	K_1	0.22	0.200	0.020	309	311.3	-2.3
	O_1	0.13	0.109	0.021	256	249.6	6.4
Kongtong Island	M_2	0.76	0.753	0.070	292	296.4	4.4
	S_2	0.19	0.218	−0.028	343	351.1	−8.1
	K_1	0.14	0.144	−0.004	294	299.6	−5.6
	O_1	0.09	0.073	0.017	241	236.1	5.9

Table 4 Velocity verification

Site	Error analysis	
	RMSE	*r*
2-1	0.222	0.836
2-2	0.241	0.829
3-1	0.217	0.785
3-2	0.195	0.849
4-1	0.183	0.830

Notes: Since the stability of the flow direction cannot be evaluated at a low flow velocity, we did not analyze the error in the flow direction.

2.4 Turbine Simulation

To determine the degree to which a tidal-current-energy development project may impact the ambient environment, appropriate methods must be adopted to simulate the flow-field alterations associated with the deployment of a tidal farm. At present, three approaches are commonly used to predict these changes: 1) Modification of the bottom friction coefficient in the local computational grid cells to simulate the hydrodynamic effect of resource exploitation (Blunden and Bahaj, 2006; Wu *et al.*, 2013). However, this method is difficult to apply to three-dimensional models (Baston *et al.*, 2015). 2) The addition of a source term of momentum loss to the model's governing equations to simulate the energy-extraction flow field (Chen *et al.*, 2015; Wu *et al.*, 2017). 3) Adjusting the parameters of the local turbulence model to simulate the between the energy extraction and baseline cases.

The differences in the water level (Fig.9) show that the exploitation of resources by the assumed tidal farm would have some impacts on larger areas of open water, with a maximum fluctuation in the water level of less than 6 cm, which was slightly greater than that predicted by Wu *et al.* (2013). The water level fluctuation near Hailv Island (located in the north of Chengshan Cape, as shown in Fig.2) was relatively visible, and would reach 10 cm.

In addition, the difference in the flow velocity (Fig.10) reveals that the flow velocity in the wake of the farm would drop significantly, with a potential maximum drop of more than 0.8 m s^{-1}, and the range of this impact would extend 10 km downstream. Due to the blockade effect, there would be a clear increase in the flow velocity on both sides of the farm, especially on the side near land, which might aggravate the erosion of the coast. The farm might also have an impact on the flow field around Hailv Island, especially during ebb tide.

Based on the results of our analysis, the assumed tidal farm and its corresponding current development intensity might dramatically change the tidal characteristics around Hailv Island (Fig.2). As a natural scenic spot, this island is home to a large number of water birds, so the farm may greatly impact its ecological environment. Therefore, it is of great importance to incorporate technical feasibility and environmental tolerance in any tidal energy development.

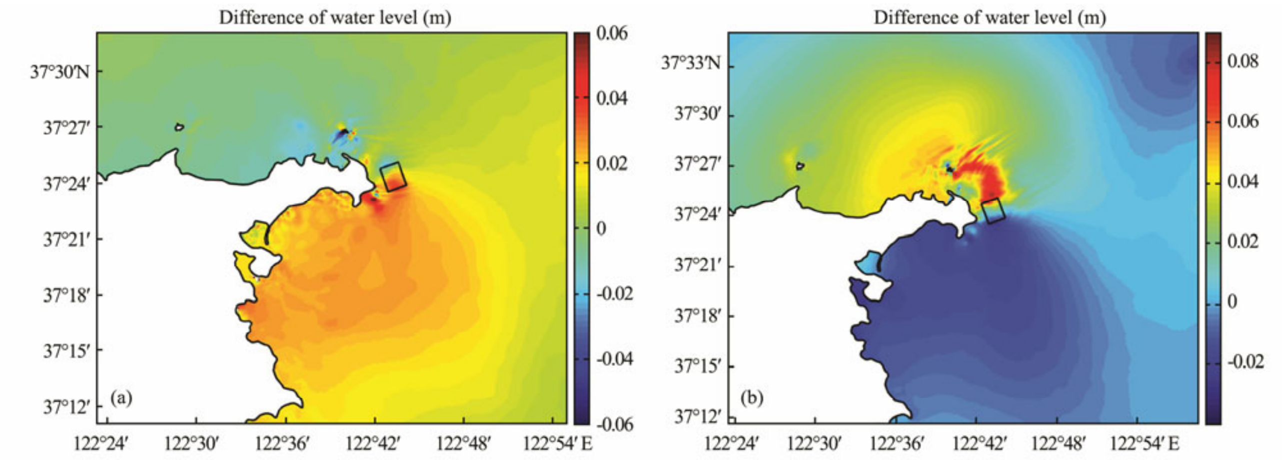

Fig.9 Difference in the water level during spring-flood (a) and spring-ebb (b).

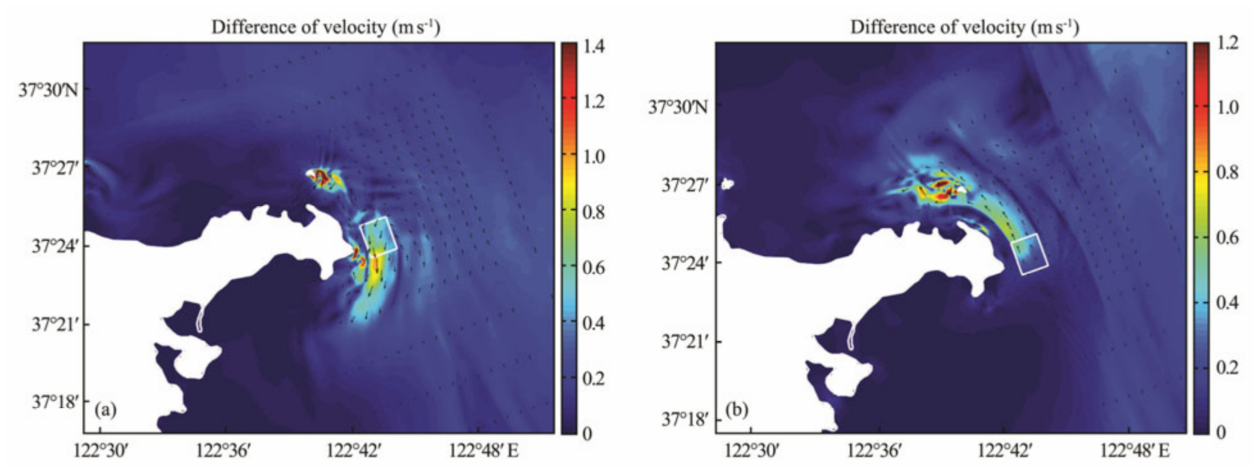

Fig.10 Difference in the velocity during spring flood (a) and spring ebb (b) tides.

4 Conclusions

In this paper, we described our construction of a hydrodynamic model of the waters near Chengshan Cape using the Delft3D-Flow module. We then described our numerical simulation of the potential influences of the exploitation of tidal current energy in the sea area by the incorporation of a given tidal farm into the model, wherein the momentum losses in the relevant nodes of the model's computational grids were equalized where the flow passed the turbines. By doing so, it was possible to evaluate the impacts of the farm on the surrounding waters.

In this simulation process, preliminarily plans and arrangements were established for a tidal farm consisting of 480 turbines in the water, each with a diameter of 25 m, by comprehensively weighing the *TSE* index, water depth and other values. Based on our analysis of the simulated data, we estimated the power output of the farm to be approximately 20.34 MW. Then, we evaluated the impacts of the farm on the water level and flow velocity in nearby waters. According to the simulation results, the impact on the water level in the area would be relatively large, with the maximum water level change of around 6 cm. The maximum flow velocity in the farm's wake would drop by more than 0.8 m s^{-1}, and the influence range would extend 10 kilometers downstream. In addition, the farm operation could change the flow field near Hailv Island, so its explicit environmental impacts require further investigation and consideration.

Acknowledgements

This study was supported by the National Natural Science Foundation of China (No. 51479185), and the Major Basic Research Project of Shandong Province (No. ZR 2017ZA0202). The authors are grateful for the provision of financial support.

References

Bahaj, A. S., Molland, A. F., Chaplin, J. R., and Batten, W. M. J., 2007. Power and thrust measurements of marine current turbines under various hydrodynamic flow conditions in a cavitation tunnel and a towing tank. *Renewable Energy*, **32** (3): 407-426.

Baston, S., Waldman, S., and Side, J., 2015. Modelling energy extraction in tidal flows. *TeraWatt Position Paper.* Revision 3.1, 1st edition, Chapter 4, MASTS, 75-107.

Black & Veatch Consulting, Ltd., 2009. Assessment of Tidal Energy Resource. *Marine Renewable Energy Guides*. European Marine Energy Centre (EMEC).

Blunden, L. S., and Bahaj, A. S., 2006. Initial evaluation of tidal stream energy resources at Portland Bill, UK. *Renewable Energy*, **31** (2): 121-132.

Chen, W. B., Liu, W. C., and Hsu, M. H., 2013. Modeling evaluation of tidal stream energy and the impacts of energy extraction on hydrodynamics in the Taiwan Strait. *Energies*, **6** (4): 2191-2203.

Chen, Y., Lin, B., Lin, J., Lin, J., and Wang, S., 2015. Effects of stream turbine array configuration on tidal current energy extraction near an island. *Computers & Geosciences*, **77** (C): 20-28.

Defne, Z., Haas, K. A., and Fritz, H. M., 2011. Numerical modeling of tidal currents and the effects of power extraction on estuarine hydrodynamics along the Georgia coast, USA. *Renewable Energy*, **36** (12): 3461-3471.

Fang, H., Bao, X., Li, B., and Liu, Q., 2015. The assessment of extactable tidal energy and the effect of tidal energy turbine deployment on the hydrodynamics in Zhoushan. *Acta Oceanologica Sinica*, **34** (5): 86-91.

Feldman, M., 2007. Tidal current energy assessment for Johnstone. *Kraftahrzeugtechnik*, **30** (2): 175-177.

Hasegawa, D., Sheng, J., Greenberg, D. A., and Thomopson, K. R., 2011. Far-field effects of tidal energy extraction in the Minas Passage on tidal circulation in the Bay of Fundy and Gulf of Maine using a nested-grid coastal circulation model. *Ocean Dynamics*, **61** (11): 1845-1868.

Iglesias, G., Sánchez, M., Carball, R., and Fernάndez, H., 2012. The TSE index – A new tool for selecting tidal stream sites in depth-limited regions. *Renewable Energy*, **48** (7): 350-357.

Li, H., Wu, G., Liang, B., and Fei, F., 2012. Numerical assessment of tidal stream energy resource in Langyatai Strait. *IEEE Oceans 2012*. Yeosu, Korea (south), 1-5.

Li, Q., 2013. Space-time distributional characteristics of wave energy and tidal current energy in Chengshantou sea area. Master thesis. Ocean University of China.

Li, Q., Zhou, L., Wu, K., Li, J., Li, Z., and Han, L., 2013. Tidal stream energy assessment on Chenshantou. *Transactions of Oceanology and Limnology*, **2013** (3): 10-18 (in Chinese).

Li, Y., Pan, D. Z., Cheng, W. L., and Pan, C. H., 2018. Tidal stream energy resource assessment in the Qiantang River Estuary, China. *International Journal of Sustainable Energy*, **37** (7): 704-717.

Mungar, S., 2014. Hydrodynamics of horizontal-axis tidal current turbines; A modelling approach based on Delft3D. Master thesis. Delft University of Technology.

Neill, S. P., Vögler, A., Goward-Brown, A. J., Baston, S., Lewis, M. J., Gillibrand, P. A., Waldman, S., and Woolf, D. K., 2017. The wave and tidal resource of Scotland. *Renewable Energy*, **114**: 3-17.

Roc, T., Greaves, D., Thyng, K. M., and Conley, D. C., 2014. Tidal turbine representation in an ocean circulation model: Towards realistic applications. *Ocean Engineering*, **78** (1): 95-111.

Waldman, S., Bastón, S., Nemalidinne, R., Chatzirodou, A., Venugopal, V., and Side, J., 2017. Implementation of tidal turbines in MIKE 3 and Delft3D models of Pentland Firth & Orkney Waters. *Ocean & Coastal Management*, **147**: 21-36.

WL Delft, 2003. *Hydraulics. Delft3D-Flow: Simulation of Multi-Dimensional Hydrodynamic Flows and Transport Phenomena, Including Sediments*. User Manual, Deltares.

Wu, H., Wang, X., and Han, L., 2013. Assessment of extractable energy of tidal current at Chengshantou Cape. *Oceanologia et Limnologia Sinica*, **44** (3): 570-576.

Wu, H., Wang, X., Wang, B., Bai, Y., and Wang, P., 2017. Evaluation of tidal stream energy and its impacts on surrounding dynamics in the eastern region of Pingtan Island, China. *Journal of Oceanology and Limnology*, **35** (6): 1319-1328.

Wu, H., Zhao, S., Xu, H., and Zhang, Z., 2010. Preliminary assessment of tidal current energy on Chengshantou area. *Ocean Technology*, **29** (3): 98-100.

Yang, L., 2012. Numerical estimates on tidal stream energy resources of the coastal areas of Shandong Peninsula. Master thesis. Ocean University of China.

(Edited by Xie Jun)